TWO COLOR REFRACTOMETRY, PRECISION STELLAR CATALOGS, AND THE ROLE OF ANOMALOUS REFRACTION

Douglas G. Currie
University of Maryland

I. INTRODUCTION

Atmospheric refraction, with its non-predictable variations, is one of the dominant sources of error in the precise determination of the apparent position of a star. It appears that this will be the dominant error source for the new generation of instrumentation now being installed for the determination of stellar catalog and Universal Time (i.e., the USNO 65-cm PZT). The effects of anomalous refraction measurements of stellar position propagate to the various quantities derived from this data. This includes the compilation of stellar catalogs, the determination of Universal Time, and variations in the latitude.

A unique instrument, the Two-Color Refractometer, can for the first time, directly measure the total deviation which the light of a star suffers due to refraction and thus can be used in a measurement program to evaluate the various aspects of anomalous refraction. In addition, this system may be used to make fundamental astrometric observations which are free from the deleterious effects of refraction.

A. Atmospheric Refraction

There are two aspects of refraction errors which are useful to discuss separately. The first of these effects are the short-term errors or the "random error" in an individual measurement. These errors affect an individual measurement so that it may be significantly different from measures made before and after it on the same night. This type of error may be of the order of 0.15 arc-seconds or larger. When we later discuss all of the errors more generally in terms of the power spectra of the anomalous zenith refraction, the random error is characterized by the magnitude of the power spectra in the domain having periods of a few minutes.

The many individual measurements may be analyzed and the results averaged together for an entire night. This procedure should result in

E. Tengström and G. Teleki (eds.), Refractional Influences in Astrometry and Geodesy, 131–155.

an improved determination of the quantities derived from the stellar position measurements. The improvement should be parameterized by a factor proportional to $1/\sqrt{n}$. This will occur if the errors of each separate measurement are independent. However, if there are phenomena which affect the anomalous refraction which have long periods, then the determination of the averaged quantities may now show this improvement. Again, discussing the question in terms of the power spectra, one will obtain the improvement in performance only if the power spectra vanishes for periods longer than a few minutes. We now address the effects of the power spectra for periods greater than the time which is required for a single observation. The systematic error to be expected may be derived from the power spectra with the period in question.

B. Derivations of Star Catalogs

We wish not to consider the question of the improvement of the star catalogs. This will require one to both improve the measurement of the single observation and reduce the systematic errors obtained when averaging data over long periods. The former will improve the basic random error and the latter will insure that the result of many measurements will reduce this diminished random error in proportion to $1/\sqrt{n}$. In general, the stellar catalog measurement using the Transit Circle is not affected by three types of error. These are: the anomalous refraction, the encoder errors, and the lack of stability of the personal equations. It is difficult to separate the effects of these errors prior to the measurements of anomalous refraction. Therefore, we shall address the remaining remarks to measurements made with the Photographic Zenith Tube (PZT). For the PZT, the errors of encoders and lack of reproducibility of personal equation are far less significant than in the Transit Circle. In addition, to first order one is independent of normal refraction and only sensitive to the anomalous refraction. In this discussion, we refer to the "normal refraction" as that theoretical quantity derived from the zenith distance of the star, and the local pressure, temperature, and humidity. The anomalous refraction is the difference between this normal or calculated refraction and the actual measured refraction.

In the case of the PZT, the normal random error is of the order of 0.18 arc-seconds. This is the internal precision for one night and does not include the effects of longer period phenomena which is probably significantly smaller. It is more difficult to estimate the errors with a longer period. These effects, due to phenomena like the heat island effect of Washington, D. C., the seasonal variation of the heat island effect, and long term weather effects may lead to violation of the horizontal uniformity which is assumed in the normal data reduction procedure. The derivation of the averaged measures for one night at the USNO may be of the order of 0.06 arc-seconds for periods between one and one hundred days.

C. Two-Color Refractometer

In order to address the role of anomalous refraction in these determinations of star position, we suggest the development and use of the Two-Color Refractometer (TCR). The TCR is a system which measures the magnitude of the refraction due to the atmosphere when observing a star. This measurement is not affected by problems of an encoder, a star catalog, or variations in personal equation. It is a measurement which isolates the refraction alone.

The primary subsystem of the Two Color Refractometer is the Quadrant Sensor System (QSS). The QSS is an operating system which has been developed at the University of Maryland. The QSS is an "eyepiece" which permits one to determine the apparent star position with great accuracy. This determination of the apparent direction to the star is performed by observing in two different colors. Using a knowledge of the index of the refraction and the dispersion of the air, one may compute from this data the instantaneous magnitude of the angle of refraction. Using the local temperature, pressure, and humidity, one may then compute the normal refraction. The difference between the normal angle of refraction and the measured angle of refraction is the anomalous refraction. The latter will be done by exactly the same calculation which is normally used by USNO for the reduction of transit circle observations.

In general, the anomalous refraction will depend upon both zenith distance and time. Let us for the moment neglect the time variation. Then a number of stars may be observed "at one instant" (actually a period of about thirty minutes). The measured value of the anomalous refraction may then be expressed in a power series function about the zenith in terms of "east" and "north" direction. The first term, which will be a constant term, which might be due to the use of erroneous values of local pressure, temperature and humidity, for the computation of the normal refractions. Any linear terms which appear would be due to gradients in the atmosphere. Quadratic terms should be small if the theory is proper and the constant term is not large.

II. OPERATION AND PERFORMANCE OF QUADRANT SENSOR SYSTEM

In this section we consider an ideal Quadrant Sensor System (QSS) and discuss the expected performance of such a system. The objective of the first part of this section is to define the type of sensor system which would be most desirable and to provide a model for the performance analysis which will appear later in this section. The realization of the QSS system will be discussed in Section IV.

The QSS system is based upon a special photosensor, the "Quadrant Photo Sensor" produce by the Electronic Vision Company, a division of

https://doi.org/10.1017/S0074180900065943 Published online by Cambridge University Press

Science Applications, Inc. The Quadrant Photo Sensor (QPS) consists of a quadrant silicon diode which is mounted in an evacuated envelope. Photons are converted to photoelectrons at the photocathode and accelerated electrostatically to an energy of 15 KeV. They are then electrostatically imaged onto the quadrant diode. The overall mechanical configuration of the Quadrant Photo Sensor (QPS) is illustrated in Figure 1.

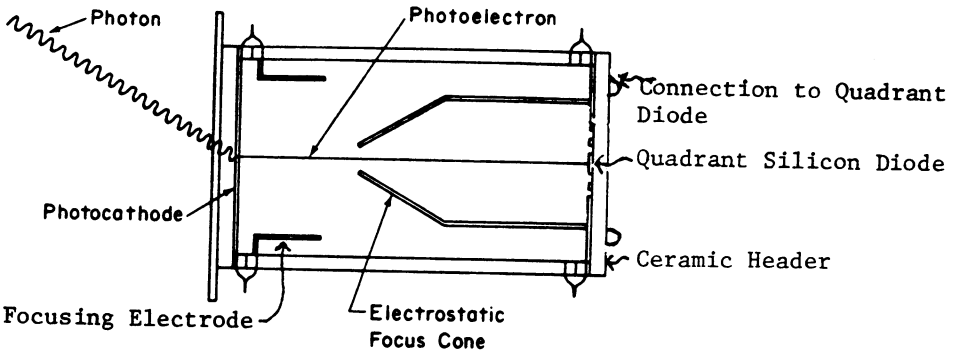

Schematic Diagram of Quadrant Photo Sensor
Figure 1

The photoelectron, which is accelerated to 15 KV, produces extensive ionization within the silicon in the photodiode. The output of a photodiode which is bombarded by a single photoelectron is a charge packet which consists, at the normal operating voltage, of about 2,000 electrons. This pulse signal generated by this charge packet is amplified, shaped, and finally detected with a level discriminator. In order to operate such a system, we wish to provide functions indicated in Figure 2.

Thus Figure 2 illustrates the photon detection system, which provides a high-level pulse for the arrive of each photoelectron. By accumulating these counts, one would have available the intergal number of counts for any interval. However, we wish to use such a system in several applications where a greater variety of outputs are required. The above system will be used as the basis for the calculations presented in Section II. At present, however, we shall now continue this discussion to describe the full Quadrant Sensor System requirements. The subsystem described

https://doi.org/10.1017/S0074180900065943 Published online by Cambridge University Press

in Figure 2 is connected to a data processing subsystem.

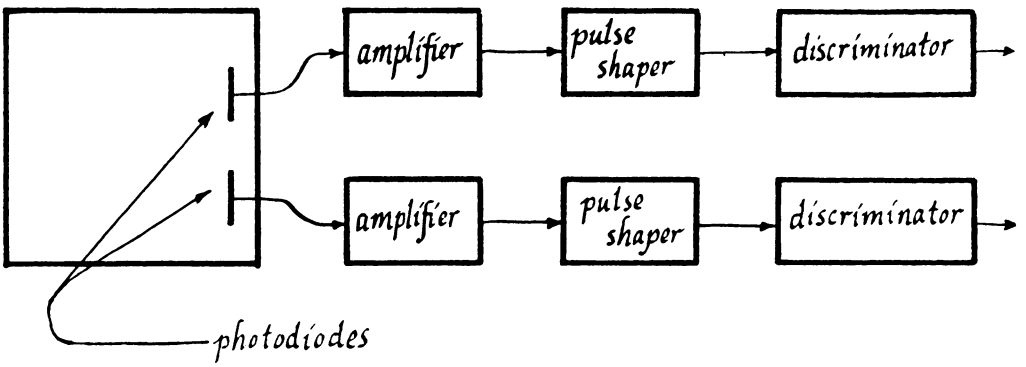

QSS Detection Subsystem for Single Photoelectrons
Two of the Four Channels are Shown
Figure 2

Thus Figure 2 illustrates the photon detection system which provides a high-level pulse for the arrival of each photoelectron. By accumulating these counts, one would have available the intergal number of counts for any interval. However, we wish to use such a system in several applications where a greater variety of outputs are required. The above system will be used as the basis for the calculations presented in Section II. At present, however, we shall now continue this discussion to describe in Figure 2 is connected to data processing subsystem.

The QSS has been designed both to provide the input for a telescope used for tracking of stars, but also to detect laser returns from satellites and track on these returns. However, the latter function is not used in this application and will not further be considered.

When operating in the photon sensing mode, the system is expected to produce an output signal which is proportional either to the intergal number of counts or the count rate smoothed in some fashion. Two outputs of this type, which are the difference between the counts from each axis, are available (X high pass, Y high pass). In addition, the output is then filtered with a low pass filter having a time constant of about 1 second. This is available as $X_{\text{low pass}}$ and $Y_{\text{low pass}}$. The high speed outputs will be used as the input or an external subystem to stabilize the image with a high frequency response. The low frequency output will provide the signals required to move the telescope. The signals described above are available in analog form in order to operate the analog servo-loops. They are also multiplexed onto an A-to-D Conver-

https://doi.org/10.1017/S0074180900065943 Published online by Cambridge University Press

ter to provide outputs which may be used for computer control and recording recording. Thus this unit is capable of both stabilizing the image, and through the photon counts, provide interval number of counts in the various channels.

In this discussion, we shall evaluate some of the numerical performance parameters for the quadrant sensor. In this section we shall presume the use of a quadrant photon counting sensor. We will assume that the photocathode has a uniform quantum efficiency and that the electronics system imposes no rate limits. The description of the actual sensor and its limitations appears in a later section.

A. Photon Noise in Direct Mode

In this section we shall compute the photon noise which affects the determination of the centroid of an image by a Quadrant Sensing System. For pedigogical ease, we hall first consider a stellar image which is square, so the brightness has the form indicated in Figure 3.

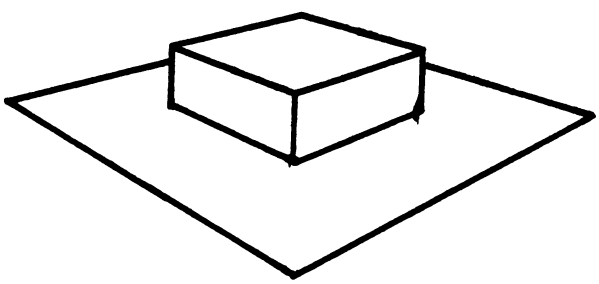

Brightness of Stellar Image
Figure 3

The difference between the performance criteria for this approximation to the stellar image (by a square pillbox) and a more realistic approximation, i.e., a Gaussian or a Lorentzian form, will be discussed later. The more realistic forms will result in about a 2% modification of the numerical results obtained for the squre pillbox image.

The results shall be expressed in terms of the total number of photoelectrons which arrive on all four quadrants (denoted by the symbol N) during a time interval denoted by the symbol T. The full width

https://doi.org/10.1017/S0074180900065943 Published online by Cambridge University Press

of the image described in Figure 3 in denoted d, which might typically have a value of two arc-seconds for a reasonable telescope used at a good astronomical site. The one dimensional projection of such an image has the form indicated in Figure 4.

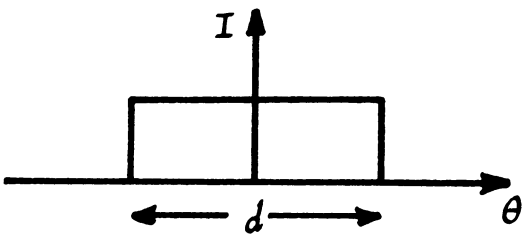

One Dimensional Projection of Square Pillbox Image
Figure 4

The number of photoelectrons per linear arc-second at the center of the square image, denoted by $\tilde{N}$, is given by

$$\tilde{N} = N/d = N/(d_o\sqrt{3}) \qquad \text{(II.A.1)}$$

where d_o is the "rms diameter". This quantity is obtained by doubling the rms radius, which is the deviation of the light intensity distrition over the image plane. We may reexpress $\tilde{N}$ in the form

$$\tilde{N} = (\eta N)/(2d_o) \qquad \text{(II.A.2)}$$

where we have defined the symbol η to represent a numerical coefficient which is related to the shape of the image. Thus from the above expressions, we see that for a square image

$$\eta_s = 2/\sqrt{3} = 1.547 \qquad \text{(II.A.3)}$$

Now we consider an image with a more realistic profile, i.e., a Guassian. The one dimension projection of such an image is indicated in Figure 5.

https://doi.org/10.1017/S0074180900065943 Published online by Cambridge University Press

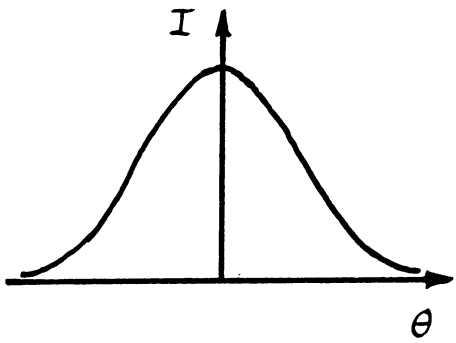

One Dimensional Projection of Gaussian Image
Figure 5

The intensity $\tilde{N}$, expressed as the number of photoelectrons/arc-seconds, has the form

$$\tilde{N}(x) = \frac{\sqrt{2}\,N}{\sqrt{\pi}\,d_o} e^{-2x^2/d_o^2} \qquad \text{(II.A.4)}$$

Thus at origin

$$\tilde{N} = \tilde{N}(o) = \frac{\sqrt{2}\,N}{\sqrt{\pi}\,d_o} = \eta_g N/2d_o \qquad \text{(II.A.5)}$$

Where we have again used the coefficient as η . Thus for the Gaussian we have

$$\eta_g = (2\sqrt{2})/\sqrt{\pi} = 1.5958 \qquad \text{(II.A.6)}$$

Thus in general, the value of η will be dictated by the model for the seeing disk, or from a more pragmatic viewpoint, from an actual measurement of the size and profile of seeing disk.

https://doi.org/10.1017/S0074180900065943 Published online by Cambridge University Press

We may later take into account a large deflection or error in image position by expressing η as a function of the offset of the image. Thus if there is an average offset of Δ , then η (Δ) will have a smaller value. In this way we will be able to address some problems which will arise in the two color application. Thus for a Guassian image

$$\eta(\Delta) = \frac{2\sqrt{2}}{\sqrt{\pi}} e^{-2\Delta^2/d_o^2} \qquad \text{(II.A.7)}$$

The quantity $\tilde{N}$ is physically related to the change in signal or differential count rate motion of the image. Thus if we apply a sinusoidal offset or a "dither" to the position by an optical device, we will see a similar variation in $\tilde{N}$. This will obviously be related to the profile, as expressed by η . On the other hand, if we assume a profile, we may invert this relation and use the measured value of $\tilde{N}$ which is obtained by applyling a dither to the servo-system to evaluate the seeing disk diameter, using the expression

$$d_o = \eta N/2\tilde{N} \qquad \text{(II.A.8)}$$

If the image is nominally centered, then a small image offset which is parameterized by the value of will result in a difference in count rates which is given by:

$$\Delta N = N_L - N_R = (N_{Lo} + \tilde{N}\cdot\Theta) - (N_{Ro} - \tilde{N}\cdot\Theta) \qquad \text{(II.A.9)}$$

We will describe the one-dimensional case. If the image was initially centered and the quantum efficiencies of the effective areas of the photocathode are equal then $N_{Lo} = N_{Ro}$ and the above equation becomes

$$\Delta N = 2\tilde{N}\Theta = \eta N\Theta/d_o \qquad \text{(II.A.10)}$$

which may be reexpressed as

$$\Delta N/N = \eta\,\Theta/d_o \qquad \text{(II.A.11)}$$

or using ΔN to compute the offset angle

$$\Theta = (\Delta N/N)\, d_o/\eta \qquad \text{(II.A.12)}$$

https://doi.org/10.1017/S0074180900065943 Published online by Cambridge University Press

We may now define a relative angle which is expressed in terms of the image diameter, so we have

$$\alpha/d_o = \Delta N/N\eta \qquad \text{(II.A.13)}$$

This expresses the angular offset due to an inequality in counts as a dimensionless angle.

Now let us determine the standard deviation of the angular position due to shot noise, i.e., the statistical error in the determination of the centroid due to the photon statistics. In each pair of quadrants (presuming we sum the photocounts from both quadrants of each side to determine the error) the mean value is

$$\bar{N}_L = \bar{N}_R = N/2 \qquad \text{(II.A.14)}$$

Thus for large value of N, the statistical noise in the value of each of these is

$$\delta N_L = \delta N_R = \sqrt{N}/2 \qquad \text{(II.A.15)}$$

Since the statistical noise in each of these quantities are independent, we have

$$\delta N = \sqrt{(\delta N_L)^2 + (\delta N_R)^2} = \sqrt{N} \qquad \text{(II.A.16)}$$

inserting this value of δN into the above expression for yields an equivalent angular offset due to the noise. Thus we have

$$\alpha = 1/\eta \sqrt{N} \qquad \text{(II.A.17)}$$

At this point, these considerations will be extended to include the effect of uniform sky background on the performance. Thus the presumed brightness now takes the form

https://doi.org/10.1017/S0074180900065943 Published online by Cambridge University Press

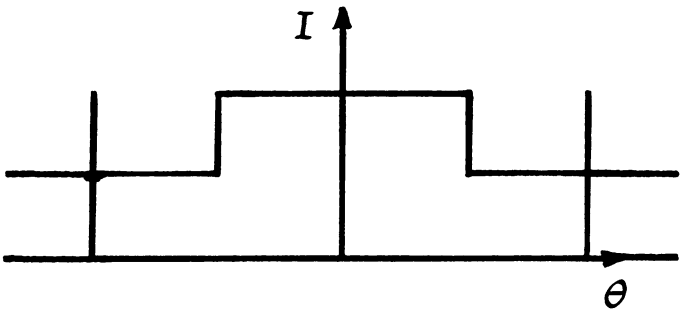

Brightness Distribution for Sky Background
With Boundard of Photosensitive Region Marked
Figure 6

where N_b is the total number of counts which appear in the four quadrants due to the brightness of the backgound sky. This is equal to the product of the field of view (in arc-seconds), the background illumination (in photoelectrons/arc-second/sec), and the integration time (in seconds). The product is expressed in photoelectrons. The image of the star is characterized as in the previous discussion. In this treatment, one simply adds the background to the image, so the mean number of counts on each side is given by

$$N_L = N_R = (N + N_b)/2 \qquad \text{(II.A.18)}$$

Thus the photon shot noise is one of the pairs of quadrants (again for relatively large signals) is given by:

$$\delta N_L = \sqrt{N_L} = \sqrt{(N + N_b)/2} \qquad \text{(II.A.19)}$$

and the values for N_R and δN_R have similar expressions. Now if we take the difference of these two independent qualities and use this quantity to determine the apparent error in pointing angles, with the presumption that the photon statistics on the two sides are independent and the sky illumination is spacially uniform, we have

$$\Delta N = \sqrt{N + N_b} \qquad \text{(II.A.20)}$$

Thus for α we have

$$\alpha = \sqrt{N + N_b}/\eta N = \sqrt{1 + (N_b/N)}/\eta\sqrt{N} \qquad \text{(II.A.21)}$$

https://doi.org/10.1017/S0074180900065943 Published online by Cambridge University Press

where we have used the total counts for the noise in the numeration, and the counts in the image for the signal which appears in the denominator. We have two types of behaviour of interest, the first of which consists of the case when the background is negligible. For this case the error becomes

$$\alpha = 1/\eta \sqrt{N} \qquad \text{(II.A.22)}$$

as discussed earlier. This is illustrated for the case of a Gaussian image in Figure 5 by the solid line.

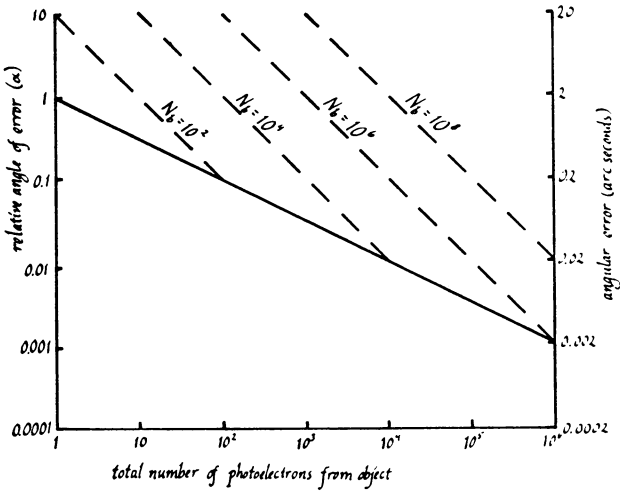

Figure 7

The other extreme case is when there is a high level of background illumination. This might represent observations conducted in the daytime with a blue sky. In this case we have:

$$\alpha = \sqrt{N_b}/N \;/\; \eta N = \sqrt{N_b} \;/\; \eta N \qquad \text{(II.A.23)}$$

This may be summarized in graphical form by the dashed line in Figure 7.

Thus Figure 7 indicated the performance that one may expect to obtain with the quadrant sensor. The expected error in the relative angle and the expected error in arc-seconds, presuming a seeing disc diameter of two arc-seconds are related to the total number of photoelectrons received during the observation period.

https://doi.org/10.1017/S0074180900065943 Published online by Cambridge University Press

We may now tranform this relationship to describe the behavior with respect to stellar brightness and telescope aperture. Let us, for example, consider a 48-inch telescope and photoelectron count rates which are caused by a particular stellar brightness for a G-2 star (or solar reflection from a satellite). We assume a quadi- S-20 photocathode as measured for a tube of this type and six mirrors with reflectivities of 0.7, 0.7, 0.86, 0.86, 0.86, and 0.86. Thus for the case of a Guassian image with negligible sky background we have the relation indicated in Figure 8.

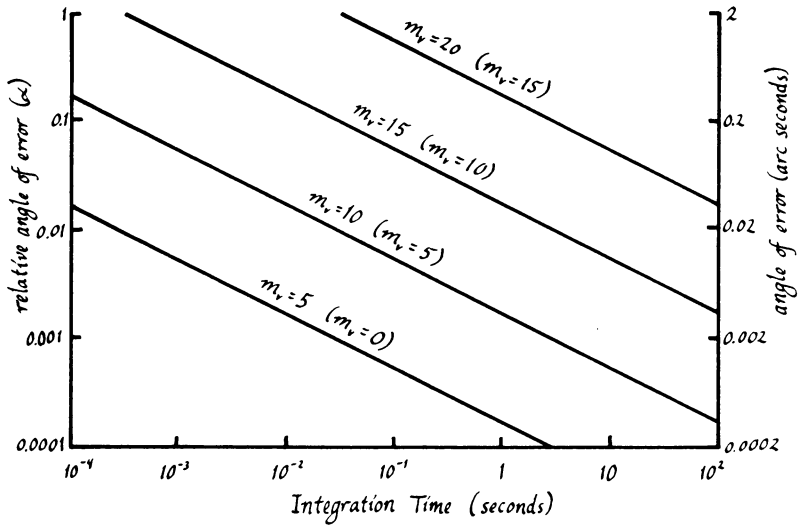

Figure 8

This indicated the ability to go to rather faint objects and still have very small angular errors due to the photon counting. The numbers in parentheses indicate the results for a 4.8-inch aperture.

III. TWO COLOR APPLICATIONS

The Quadrant Sensor System, as a component of the Two-Color Refractometer system may be used to obtain high accuracy measurements in absolute astrometry. In particular, it will determine the deviation in the apparent star position caused by the earth's atmosphere. As star light enters the earth's atmosphere, the deviation of index of refraction of the atmosphere from that of the vacuum results in a change in the direction of propagation. For a flat, horizontally-stratified atmosphere, this change in direction is a known function of the index of refraction of the air in the immediate vicinity of the telescope (the local index of refraction). This may be determined from the local temperature, pressure and humidity. However, if there are horizontal inhomogeneities,

https://doi.org/10.1017/S0074180900065943 Published online by Cambridge University Press

this change of propogation direction can not be predicted from a measurement of local surface conditions. In this section, we address a procedure to determine the magnitude of this change in direction (the "angle of refraction") from measurements made on the light of the star using the Quadrant Sensor System.

We take advantage of the fact that the magnitude of the angle of refraction depends upon wavelength, due to the dispersion of the index of refraction of air. Thus by measuring the apparent position of the star as viewed in red and in blue light, the difference in apparent position may be evaluated. This dispersion angle may be used with a knowledge of the dispersion in the index of refraction to determine the angle of refraction. Thus using the dispersion angle between the red and blue images, and the known dispersion of the air, we may determine the deviation of the direction of propogation of the starlight due to the atmosphere.

In order to illustrate the operation of the Two-Color Refractometer (TCR) let us consider the basic relations governing the refraction. The symbol Θ_λ describes the deviation of a ray of wavelength λ from its initial direction and ϕ is the true zenith distance of the star. The index of refraction of the air at the wavelength λ is denoted by n_λ. Thus from Snell's law, we have

$$\Theta_\lambda = (n_\lambda - 1)\phi/n_\lambda \quad . \qquad \text{(III.1)}$$

Since n_λ is very close to unity, we shall approximate this expression by:

$$\Theta_\lambda = (n_\lambda - 1)\,\phi \qquad \text{(III.2)}$$

where the definition of these quantities may be seen in the following figure

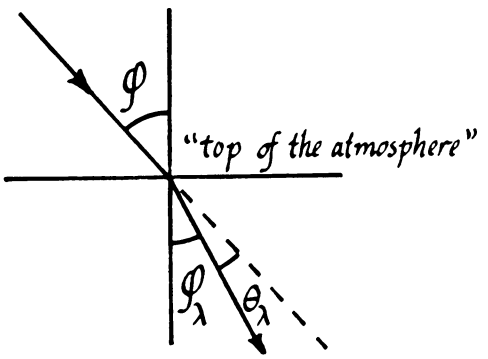

Effect of Refraction on Starlight
Figure 9

https://doi.org/10.1017/S0074180900065943 Published online by Cambridge University Press

While the figure illustrates a simple idealized case, a little reflection indicates that equations apply to the more general case of a continuously variable, non stratified, spherical atmosphere. For the calculation made in the later part of this section, we use the following expression for the index of refraction for dry air

$$(\eta_\lambda - 1) \times 10^{-6} = 64.328 + 29498.1\ (146 - \lambda_0^{-2})^{-1} + 255.4\ (41 - \lambda_0^{-2})^{-1} \qquad \text{(III.3)}$$

This applies for a temperature of 15°C, a pressure of 760 mm and no water vapor. This expression is not the optimal form for expressing the index of refraction when reducing the data for the operational system, but it is entirely satisfactory for the system analysis and error analysis presented in this section.

In order to permit the independent variation of the wavelength selected for obervation within a reasonable error analysis, we shall use the blue and red measurements and a parameter which depends on the wavelengths used to determine the magnitude for the angle of refraction at a reference wavelength chosen to be the center of the visual band (5600Å). Thus for the wavelengths at which we will measure the relative angular position, we use:

$$\Theta_R = (\eta_R - 1)\,\phi \qquad \text{(III.4)}$$

$$\Theta_B = (\eta_B - 1)\,\phi \qquad \text{(III.5)}$$

We will then use these expressions to determine the zenith distance ϕ, which we will relate to the angle of refraction in the green by the relation

$$\Theta_V = (\eta_V - 1)\,\phi \qquad \text{(III.6)}$$

Thus we will determine the angle of refraction in the visual band. This particular equation does not appear to represent the optimal procedure for minimizing the propogation of experimental errors but we shall use it as a useful tool for system analysis. Thus we obtain an expression of the form:

$$\Theta_V = \Omega\,(\Theta_B - \Theta_R) \qquad \text{(III.7)}$$

https://doi.org/10.1017/S0074180900065943 Published online by Cambridge University Press

where

$$\Omega = (\eta_V - 1)/[(\eta_B - 1) - (\eta_R - 1)] \qquad \text{(III.8)}$$

If we measure the difference in apparent angular position of the blue and the red image, this angular difference, multiplied by the quantity Ω, will yield the angle of refraction suffered by the visible light. This is the value for local conditions which are 15°C and a pressure of 760 mm Hg.

In order to provide a general frame of reference, let us consider the numerical values for the refraction and the dispersion angles. Let us consider the value of for various choices of the limiting wavelengths. We have

Effective Blue Wavelength	Effective Red Wavelength	Ω
3500Å	6000Å	30.36
3300Å	6000Å	25.27
3500Å	7000Å	26.89

Relation Between Selected Wavelengths and Ω Multiplier
Table 1

Since the eventual error is proportional to the value of Ω, we would prefer the smallest possible value. From Table 1 we see that the value of Ω decreases and thus the error multiplier decreases as the spread between the wavelengths increase. This dependence is particularly sensitive to the wavelength of the blue observation where a change of 200Å provides as much improvement in Ω as a change of 1000Å in the wavelength of the red observation. However, for various technical reasons we will accept the first case as a reasonable, practical limit.

Let us now evaluate the sources of error in this determination. Differentiating the expression for Θ_v, we have:

$$\delta\Theta_V = \frac{\delta\Omega}{\Omega}\,\Theta_V + \Omega\,(\delta\Theta_B - \delta\Theta_R) \qquad \text{(III.9)}$$

We now presume the uncertainty in the measurement of the angular position of the image in the red and in the blue have the same magnitude,

https://doi.org/10.1017/S0074180900065943 Published online by Cambridge University Press

and are independent. Concerning the former, it assumes similar filter widths which will probably not be the case, but it is a useful point for discussion. Thus for the part of the variation due to uncertainty in angular measurement we have

$$\delta\Theta_V \quad \sqrt{2}\ \Omega \quad \delta\Theta \tag{III.10}$$

where

$$\delta\Theta = \delta\Theta_B = \delta\Theta_R \tag{III.11}$$

We may now use the relations between the total number of counts and angular errors to express the accuracy of the determination of $\delta\Theta_V$ as a function of the total number of photoelectrons. In Figure 10 we have also indicated the various system operating points obtained when the QSS is running at the maximum count rate (the normal procedure) for various intervals to time. These results include the effect of the UV filter and the red filter.

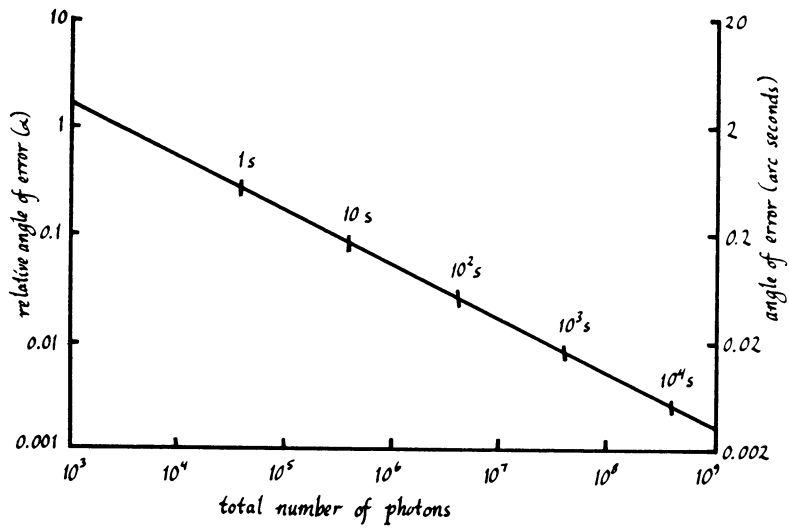

Relation Between Total Number of Counts and Error in Anomalous Refraction for TCR
Figure 10

https://doi.org/10.1017/S0074180900065943 Published online by Cambridge University Press

We now consider the other source of error which appeared in the Equation for $\delta\Theta_V$. This is the possible variation in the quantity Ω. It is presumed that Ω is calculated for the local value of refraction (i.e. using pressure and temperature). The predominant remaining reason for an controlled uncertainty in $\delta\Theta_V$ is due to the variable water vapor content in the atmosphere. In order to evaluate this phenomenon, the following table is presented. This presents the value of Ω and the change produced in Ω due to precipitable water for various pairs of effective wavelengths. We use the mean water vapor which is expressed in the terms of precipitable water vapor (for a flat atmosphere).

Effective Wavelength for Blue Filter	Effective Wavelength for Red Filter	Ω for no Water	Precipitable H_2O	Ω with Water Vapor	$\delta\Theta/\Omega$
3500	6000	30.3657	10 mm	30.1885	0.0058
3300	6000	25.2696	10 mm	25.1232	0.0058
3500	7000	26.8927	10 mm	26.7351	0.0059
3500	6000	30.3479	1 mm	--	0.00065

The Effect of Water Vapor on Systematic Errors
Table 2

Thus we see that the water vapor correction is approximately proportional to the amount of water and generally independent of the selection of the effective wavelength of the filters.

Let us now consider a numerical example. If we observe a star at zenith distance of 30° as one might with an astrolabe, then using the expression for the refraction under standard temperature and pressure

$$\Theta_V = 58''.2 \tan Z \qquad \text{(III.12)}$$

which applies to a flat atmosphere we have, at 30°, a deflection of about 34". If we wish to be able to determine this correction with an accuracy of 0".05, then we need

$$\frac{\delta\Theta_V}{\Theta_V} = \frac{\delta\Omega}{\Omega} = \frac{0''.05}{33''.6} = 0.0015 \qquad \text{(III.13)}$$

https://doi.org/10.1017/S0074180900065943 Published online by Cambridge University Press

This means one to know the water content to 2.3 mm of precipitable water.

However, this requirement is not particularly difficult since commercially available microwave ratiometer are accurate to about 1 or 2 mm of precipitable water. In addition, a system attached to the TCR using near IR measurements in and out of a water absorption band should be significantly more accurate and less complicated.

A. Some Practical Considerations

We now consider a few practicle aspects of the design of the TCR. The full discussion of the system will be considered at a later time.

We first consider the procedure for sampling the light at two different colors. One might attempt to measure the position of the red and blue images at the same time with two different quadrant sensor. The parameters which enter Figure 6 are based upon this assumption. However, a more practical approach to this problem is to use a single quadrant sensor. The detailed reasons will be considered in a separate discussion. We shall, briefly, discuss this approach and how we should use it to maximize the accuracy of the evaluation. Thus we note that due to the fact that the refraction in the atmosphere has significant power at various frequencies, one might wish to sample the two different colors continuously and at the same time. If this is done, then both the power at high frequency and the power at low frequency (the image motion) are properly tracked and do not affect the accuracy of the measurement.

However, the mechanical stability requirements strongly suggest the use of a single detector. If one switched the two colors onto the one sensor at a rate of several hundred times a second, one may show that the residual error is expected to be random and has a value of less than 0.01 arc-seconds for the measurement lasting several minutes.

The remaining uncertainty is in the determination of the water vapor. From the previous discussion, and typical values of water vapor to be expected, this effect may be totally ignored for the initial measurements out to a distance of 15° from the zenith.

B. Expected Accuracy for Measurements of Zenith Refraction

We now discuss the accuracy which we would expect to obtain with measurements using this instrument. These will be expressed in terms of the measurement errors to be expected on the power spectral density, and will be based upon use of the 48-inch telescope at the Goddard Optical Research Facility (GORF). However, approximately the same numbers apply to the set of measurements which would be performed on the 36-inch telescope. For these evaluations, we will presume the use of the present circuit for the quadrant sensor which has a maximum counting

https://doi.org/10.1017/S0074180900065943 Published online by Cambridge University Press

rate of 10 kilohertz/quadrant. This will permit the observation of 8th magnitude stars with the proper count rate. Since we will limit our measurements to a region that is between 5 and 10 degrees, it is worth noting that we would statistically expect to have about 80 stars within a five degree circle of the zenith.

In general, the relationship between the stellar magnitude, the telescope aperture and the expected photon statistical error for a ten minute observation is expressed in Figure 11.

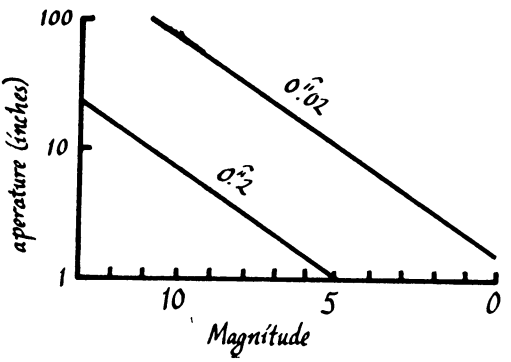

Figure 11

Combining the results of Figure 10 and Figure 11, we see that we may trade off between the aperture size of the telescope with the observing time to use a small telescope and still have a reasonable number of stars to observe.

Now presuming this count rate, we can evaluate the power spectrum of the system errors which we expect. To facilitate this present discussion, we will not consider the true power spectrum but indicate the standard deviation of the system error for a measurement of a given length. The overall results are thus summarized in Figure 12. The system error caused by the photon statistical noise is illustrated by the broad solid line. For periods shorter than one second, one may increase the centroid of the white light image and rely on the smoothness of the telescope tracking to determine the refraction (called image in this domain) rather than the two-color extraction. This is expected, with some study of the records and knowledge of the telescope, to give about 0".2. If these measurements were conducted on the 100-inch telescope at Mt. Wilson, which has a very smooth and regular drive, and were conducted on a night of low wind, this system error could probably be reduced to 0.1 arc-seconds. For periods of more than 10 seconds, however, one would expect that errors in the telescope drive will become too large. In order to study the behavior for longer characteristic times, we consider a limit for a single observation of twenty

https://doi.org/10.1017/S0074180900065943 Published online by Cambridge University Press

minutes which results in an error of 0.01 arc-seconds. Thus one might expect to obtain an increase in accuracy by about a factor of three, but this will mean the observation of new stars. The feasible accuracy in this region must be more carefully explored. For the longer period term, one averages the data obtained on successive nights to obtain these results. However, since we do not expect to observe for 24 hours a day, there is a break in this curve as one goes to the dashed portion. Presuming an observation period of two hours for a night, we obtain the dashed curve. At about 0.03 arc-seconds one expects to run into systematic errors. It seems possible that these may be calibrated to the 0.001 or 0.002 arc-second level. Accuracies beyond this cannot currently be projected for the first generation instrument.

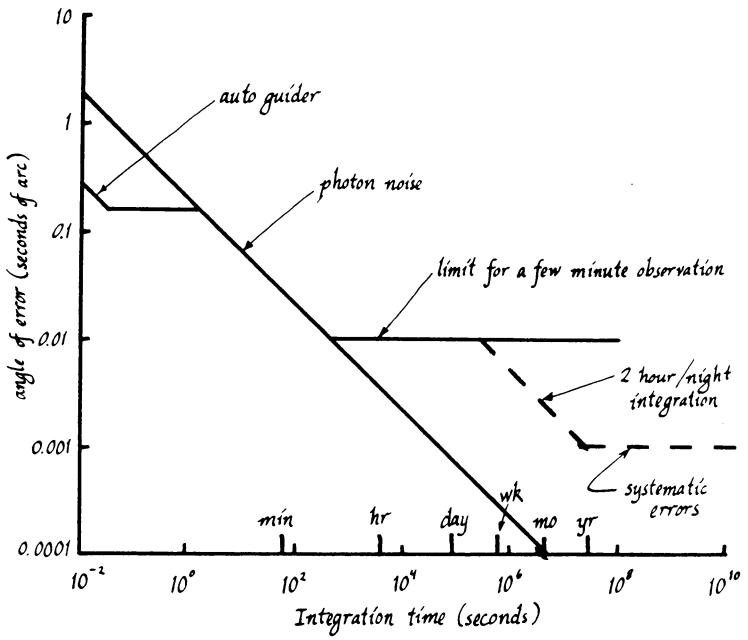

Figure 12

IV. IMPLEMENTATION OF THE QUADRANT SENSOR SYSTEM

In this section we describe the Quadrant Sensor System which has been developed within the Amplitude Interferometer Program at the University of Maryland. This system is the practical realization of the hypothetical QSS which was described in Section II. The basic element of the system consists of two standardized units, the photosensor head and the control unit which have been used in three different

https://doi.org/10.1017/S0074180900065943 Published online by Cambridge University Press

astronomical system. The quadrant sensor system is basically a special system which detects light in four channels. These are closely placed and are mechanically and geometrically rigid. In order to satisfy the system requirements, a special device has been obtained from Electronic Vision Company and an electronic system has been developed at the University of Maryland to make these observations. The requirements on this optical/electronic system demand a very high precision, electronically, optically, and mechanically, as well as a considerable amount of generality. The electronic system will permit the quadrant sensor to interface to a variety of data processing system, i.e., computers or hardwired processors.

The Photosensor head contains the Quadrant Photosil. The structure has already been indicated in Figure 4 and is shown here

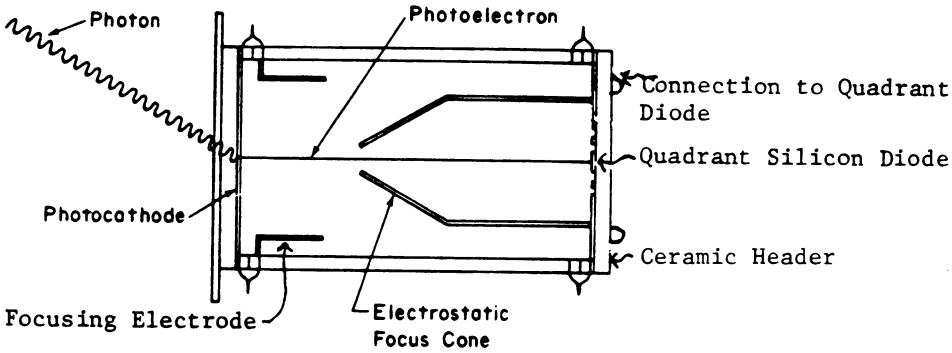

Schematic Diagram of Quadrant Photo Sensor
Figure 13

as discussed in the first section, the circuitry following the Quadrant Photosil is indicated in Figure 14

https://doi.org/10.1017/S0074180900065943 Published online by Cambridge University Press

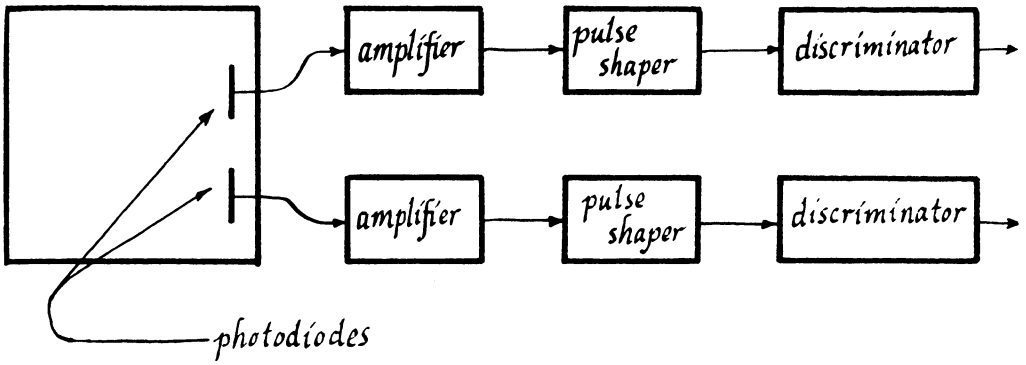

QSS Detection System for Single Photoelectrons
Two of the Four Channels are Shown
Figure 14

This results in a pulse height distribution which permits a straight-forward discriminator. The preamplifier is similar to that photon counting Digicon system developed by E. Beaver at UCSD. The pulse height distribution at 16 KV is shown in the following figure.

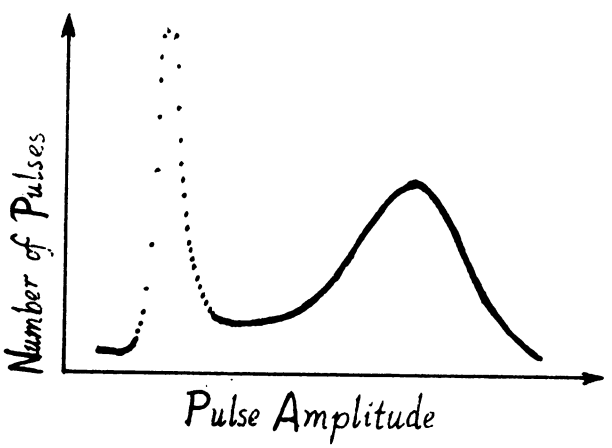

Figure 15

This system is expected to operate in environments with high levels

https://doi.org/10.1017/S0074180900065943 Published online by Cambridge University Press

of external EMI. This is a serious problem since the signals are smaller than conventional PMT's by a factor of about 1000 to 10,000.

Special shielding and grounding procedures are requried in order to prevent external TVI from interfering with the discrimination process. This has been provided for the input high voltage leads by the use of solid aluminum shields. The amplifiers are specially isolated and grounded. Even so, the pickup is noticable under certain circumstances.

The preamplifier in the QSS head provides a signal which is relatively immume to external problems. This is then sent by four short cables to the QSS Control Unit. Here the signal is reamplified and sent to discriminators. These discriminators may be adjusted independently for each of the four channels. These are normally set at about the point indicated by the arrow in Figure 15. The shape of this pulse height distribution leads to a relative immunity from effects due to the variation one expects in operating voltages and circuits in the field.

In order to interface to a computer and provide data for the closure of a servo-loop, the four signals are multiplexed and then applied to an A-to-D converter. The output is an eight-bit word. The operation acts as an asynchronous peripheral which supplied data when asked. Thus generalized system has been used in several applications. We shall now describe how it has already been used.

A. Application in Single Aperture Amplitude Interferometer

The first application of the quadrant sensor system was to provide image stabilization in Single Aperture Amplitude Interferometry (SAAI). In this system it operates in only one axis. It incorporates a device which provides high frequency stabilization with a frequency response up to about 60 hertz. The gain is set to permit the utilization of the stabilization to this level. The expected noise performance was discussed in the previous section.

As an indication of the proper performance of this system in Amplitude Interferometry, the measurements of the fringe visibility which are performed when this system is operating are significantly improved. Special procedures have been developed, both for the proper alignment of this system and to permit the simultaneous use of the manual guiding of the telescope. This is required at present since the QSS has not yet been interfaced to the large telescopes due to the necessity of performing the coordinate transformation without a computer.

B. 48-inch Telescope at the Goddard Space Flight Center

The Quadrant Sensor System (QSS) has been used to make an Automatic Guider System (AGS) to control the 48-inch telescope at the GORF. In this case, the output from the high frequency error signal is multiplexed

and digitized and fed directly to the computer. There this data on the error in pointing is processed and filtered in a digital form. This system has succeeded in providing precise pointing information and also has been useful in detecting difficulties in the encoder system. Instabilities in the computer processing of the data and the telescope setup drive can cause oscillation under some circumstances. However, the computer procedure for handling the data is now being reprogrammed to handle this properly.

In addition, the GSFC system also provides for the capability to sense the offset of lasers from a satellite reflection. To this end, the capability is provided to gate the photocathode off while the outgoing laser pulse is near the telescope with a high voltage pulse applied to a grid of a modified Quadrant Photosensor. The sensor system can detect the arrival of the laser return. The signal on each diode is amplified, and then compressed for greater dynamic range, and stores before it is presented to the multiplexer. This sequence is activated by the receipt of a photo pulse which has a value which is greater than three photoelectrons. Thus this gives the error in pointing with respect to the laser return. This system has been implemented and tested in a laboratory but the required computer programs for the 48-inch telescope and the required telescope time are not yet available in order to test the laser tracking system on the telescope.

DISCUSSION

G. Teleki: How will the observed stars, with different spectral type, influence your measurements?

D.G. Currie: answered, that because of the different spectral type of observed stars he expects some systematical effects (it is to be hoped that these effects can be determined), but the main problem is connected with the colouring of the atmosphere at different zenith distances.

J. Milewski: What a magnitude of variations (in time) of the dispersion do you expect?

D.G. Currie: answered, that he expects the variations of hundredths of arc second.

B. Garfinkel: Are you able to separate the vertical and azimuthal refractions? Do you intend to determine also the time dependence effecting only the azimuthal component of refraction or both of them?

D.G. Currie: answered the first question in the affirmative. Connected with the second question, he said that the total dependence will be examined as a function of different parameters.